

A spectroscopic study of the near-IR [SIII] lines in a sample of HII galaxies: chemical abundances

C. Kehrig^{1,2}, J.M. Vílchez¹, E. Telles², F. Cuisinier³, and E. Pérez-Montero⁴

¹ Instituto de Astrofísica de Andalucía (CSIC), Apartado 3004, 18080 Granada, Spain
e-mail: kehrig@iaa.es, jvm@iaa.es

² Observatório Nacional, Rua José Cristino, 77, 20.921-400, Rio de Janeiro - RJ, Brazil
e-mail: kehrig@on.br, etelles@on.br

³ GEMAC, Observatório do Valongo/UFRJ, Ladeira do Pedro Antônio, 43, 20.080-090 Rio de Janeiro - RJ, Brazil
e-mail: francois@ov.ufrj.br

⁴ Departamento de Física Teórica, C-XI, Universidad Autónoma de Madrid, 28049 Madrid, Spain
e-mail: enrique.perez@uam.es

Received [date]; accepted [date]; Last update August 8, 2018

ABSTRACT

Context.

Aims. A detailed spectroscopic study covering the blue to near-infrared wavelength range ($\lambda 3700 \text{ \AA} - 1 \mu\text{m}$) was performed for a sample of 34 HII galaxies in order to derive fundamental parameters for their HII regions and ionizing sources, as well as gaseous metal abundances. All the spectra included the nebular [SIII] $\lambda 9069, 9532 \text{ \AA}$ lines, given their importance in the derivation of the S/H abundance and relevant ionization diagnostics.

Methods. A systematic method was followed to correct the near-IR [SIII] line fluxes for the effects of the atmospheric transmission. A comparative analysis of the predictions of the empirical abundance indicators R_{23} and S_{23} was performed for our sample galaxies. The relative hardness of their ionizing sources was studied using the η' parameter and exploring the role played by metallicity.

Results. For 22 galaxies of the sample, a value of the electron temperature $T_e[\text{SIII}]$ was derived, along with their ionic and total S/H abundances. Their ionic and total O/H abundances were derived using direct determinations of $T_e[\text{OIII}]$. For the rest of the objects, the total S/H abundance was derived using the S_{23} calibration. The abundance range covered by our sample goes from 1/20 solar up to solar metallicity. Six galaxies present $12+\log(\text{O}/\text{H}) < 7.8$ dex. The mean S/O ratio derived in this work is $\log(\text{S}/\text{O}) = -1.68 \pm 0.20$ dex, 1σ below the solar $(\text{S}/\text{O})_\odot$ value. The S/O abundance ratio shows no significant trend with O/H over the range of abundance covered in this work, in agreement with previous findings. There is a trend for HII galaxies with lower gaseous metallicity to present harder ionizing spectra. We compared the distribution of the ionic ratios O^+/O^{++} vs. S^+/S^{++} derived for our sample with the predictions of a grid of photoionization models performed for three different stellar effective temperatures. This analysis indicates that a large fraction of galaxies in our sample seem to be ionized by extremely hard spectra, in line with recent suggestions for extra ionizing sources in HII galaxies.

Key words. ISM: abundances – ISM: HII regions – Galaxies: abundances – Galaxies: dwarf – Galaxies: evolution

1. Introduction

HII galaxies are galaxies undergoing violent star formation (Searle & Sargent 1972; Terlevich et al. 1991; Cairós et al. 2000). Their optical spectra show strong emission lines (recombination lines of hydrogen and helium, as well as forbidden lines of elements like oxygen, neon, nitrogen, sulfur, among others) that are very similar to the spectra of extragalactic HII regions. Analysis of their spectra shows that they are low-metallicity objects with the metallicity varying from $1/40Z_\odot$ to $1/2Z_\odot$ (e.g. Terlevich et al. 1991; Telles 1995 and ref-

erences therein; Vílchez & Iglesias-Páramo 1998, 2003; Thuan & Izotov 2005). Among them we can find the least chemically-evolved galaxies in the local Universe.

The study of elemental abundances in emission-line galaxies gives information about their chemical evolution and star formation history. Outside the Local Group, emission lines from ionized gas represent the principal means of deriving abundances, as energy is concentrated in a few conspicuous emission lines. Abundances for the stellar population are derived from absorption features, which are more numerous and require much higher signal-to-noise spectra to be derived meaningfully.

In HII galaxies the metal enrichment of the interstellar medium by supernovae has been operating typically in low-metallicity environments. Oxygen is the most frequently used element in deriving abundances from emission lines: abundances are easily derived, as the main ionization stages are observable in the optical range. Furthermore, oxygen is particularly suitable for chemical evolution studies, as it traces the overall metallicity very well. It originates quasi exclusively from the nucleosynthesis in type II supernovae progenitors (Meynet & Maeder 2002; Pagel 1997; Woosley & Weaver 1995). While the sources of oxygen are well-determined and the most important ionization stages can be observed in the optical range, some uncertainties still remain about the sulfur yields and its sources. In addition, not all the ionization stages can be observed in the optical range and important ionization correction factors (ICFs) must be applied to derive the total sulfur abundance. Hence comparing S and O abundances can give us some clues to sulfur nucleosynthesis and the masses of the stars where the sulfur tends to be formed.

To derive oxygen abundances, one should first derive the electron temperature, which requires the measurement of faint auroral lines, like [OIII] $\lambda 4363$ Å, which are often not detected. The alternative is to use strong line-abundance indicators, like R_{23}^1 , which calibrated empirically (Pagel et al. 1979, Pilyugin 2001) or through photoionization models (e.g. McGaugh 1991). However, the relation between R_{23} and oxygen abundance presents the noticeable drawback of being double-valued.

Vílchez & Esteban (1996) proposed S_{23}^2 as an alternative abundance indicator. In contrast to oxygen, S_{23} remains single-valued up to abundances above solar value. Furthermore, sulfur should be as useful as oxygen for tracing metallicity. From an observational point of view, S_{23} has the advantage over R_{23} that the [SII] and [SIII] lines are less affected by reddening (Pérez-Montero et al. 2005; hereinafter PM06).

To produce an accurate derivation of S/H abundance, the importance of using the nebular [SIII] lines can not be overlooked (e.g. Dennefeld & Stasińska 1983; Vílchez et al. 1988, Garnett 1989; Bresolin et al. 2004). Photoionization models indicate that S^{++} is the dominant sulfur ion (Garnett 1989; hereinafter G89), which presents three forbidden transitions at [SIII] $\lambda\lambda 9069, 9532$ Å and $\lambda 6312$ Å in the optical to near-IR (NIR) range (analogs to [OIII] $\lambda\lambda 4959, 5007$ Å and $\lambda 4363$ Å). The [SIII] $\lambda 6312$ Å line is faint, highly temperature-sensitive, and it can induce several biases in the derived S/H abundance. The NIR [SIII] lines can be quite strong, and a detailed telluric atmosphere correction has to be applied to them. Pérez-Montero & Díaz (2003) (hereinafter PMD03) and G89 derive the S^{++} ionic abundance for samples of about one dozen emission-line galaxies, both using the nebular [SIII] $\lambda 9069$ Å line. Recent work by Izotov et al. (2005) (hereinafter I05) presents S/H abundances for a large number of metal-poor emission-line galaxies from the SDSS-DR3³; how-

ever, the auroral line [SIII] $\lambda 6312$ Å was used in this work to calculate the S^{++} ionic abundance.

Here we present long-slit spectrophotometric observations of a sample of 34 HII galaxies to make a detailed analysis of their chemical abundances. The wide coverage of our spectra ($\lambda 3700$ Å - $1\mu\text{m}$) for all the galaxies in the sample provides us all the emission lines needed to estimate the oxygen and sulfur abundances directly. All the S/H abundances were estimated using a nebular [SIII] line, so that uncertainties related to the use of the auroral line [SIII] $\lambda 6312$ Å are avoided. In addition, this wavelength coverage allowed us to study the properties of the ionizing clusters of HII galaxies making use of the η' parameter and sequences of photoionization models.

In the next section we describe our sample of galaxies, the observations, and data reduction and present the line intensities. In Sect.3 we perform a comparative study between R_{23} and S_{23} abundance indicators, present an analysis about ionization structure and ionizing sources, and discuss the abundance results for the sample. Finally in Sect.4 we summarize our conclusions.

2. Data analysis

2.1. Sample and observations

The data base of this work consists of 34 intermediate-resolution spectra of HII galaxies covering a wavelength range from 3700 Å to 7000 Å (blue spectra; Kehrig et al. 2004), and from 6500 Å to $1\mu\text{m}$ (red spectra). For all the objects, measurements of the emission lines of [OII] $\lambda 3727$ Å and [SIII] $\lambda\lambda 9069, 9532$ Å exist, except for the galaxy UM151, for which we do not have a measurement of the [OII] $\lambda 3727$ Å line.

The complete log and the characteristics of the sample objects are given in Kehrig et al. (2004). The mean value for the distribution of redshifts of the sample is 0.02. Depending on the redshift of each galaxy, one of the two [SIII] lines ($\lambda 9069$ Å or $\lambda 9532$ Å) may fall in the range of telluric absorption in which atmospheric correction is critical. For this reason, this correction must be performed on a case by case basis.

Regarding the red spectra, the observations were conducted in October and December 2002 (9 nights of observations in total) with the Boller & Chivens spectrograph of the 1.52 m telescope⁴ at the European Southern Observatory (ESO), La Silla, Chile. The CCD used has a pixel size of 0.82 arcsec in spatial direction. Typical seeing of the observations was 1-1.2". All observations were performed using grating #10 with an inverse dispersion of 1.9 Å/pix, a slit width of 2.5", and a spectral range of 6000 Å - $1\mu\text{m}$. This configuration yielded an effective instrumental resolution of ~ 6 Å (FWHM) at 6000 Å. Total exposure times were typically 7200 seconds split into two exposures in order to eliminate cosmic rays during the reduction procedure.

Representative red spectra of three of the observed galaxies are shown in Fig. 1.

¹ $R_{23} = ([\text{OII}]\lambda 3727 + [\text{OIII}]\lambda\lambda 4959, 5007) / \text{H}\beta$

² $S_{23} = ([\text{SII}]\lambda\lambda 6717, 31 + [\text{SIII}]\lambda\lambda 9069, 9532) / \text{H}\beta$

³ Data Release 3 of Sloan Digital Sky Survey

⁴ operated within the agreement between Brazil and ESO

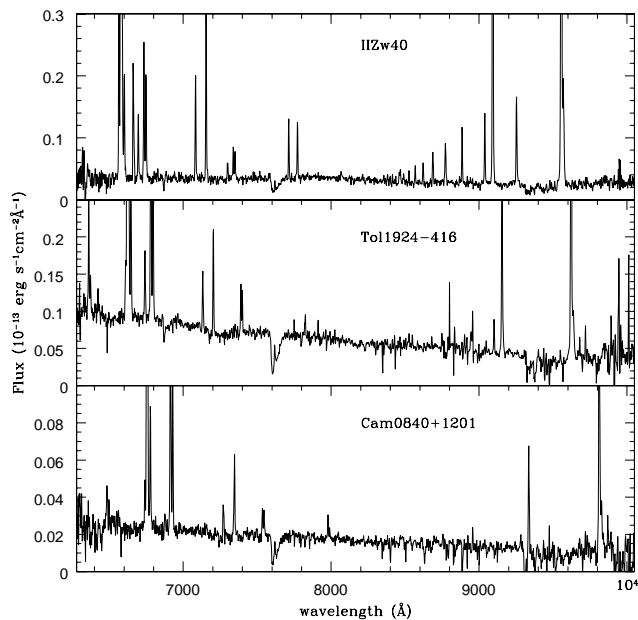


Fig. 1. Representative red spectra of galaxies of the sample.

2.2. Data reduction and telluric absorption correction

The CCD frames were reduced by employing standard IRAF⁵ packages. The spectrophotometric standard stars (~ 7 observed each night) used for flux calibration were chosen in order to have an appropriate flux-point coverage in the NIR.

Ground-based NIR spectroscopy has always been hampered by strong and variable absorption features due to the Earth's atmosphere. Even within the well-established photometric bands such as J, H, and K, telluric absorption bands are present. In analysis of the NIR sulfur emission lines, a crucial step is the correction for the effects produced by the earth's atmosphere on the spectra, especially between 8500 Å and 1 μ m (Vacca et al. 2003; Díaz et al. 1987). Exhaustive work was done to correct the whole sample for these effects. We derived, for each night, the telluric correction as a function of wavelength, $\langle f(\lambda) \rangle$, and its corresponding standard deviation, $\langle \sigma(f(\lambda)) \rangle$. A minimum of five standard stars per night was used to obtain this correction. The mean values for $\langle f(\lambda) \rangle$ and $\langle \sigma(f(\lambda)) \rangle$ are 80% and 4%, respectively. We applied the telluric correction by dividing each galaxy spectrum by its corresponding $\langle f(\lambda) \rangle$. The $\langle \sigma(f(\lambda)) \rangle$ of the correction was taken into account when calculating the overall error budget of the line fluxes.

2.3. Line intensities

The emission lines corresponding to the red spectra were measured following the same procedure as in Kehrig et al. (2004). Once the atmospheric correction was performed for each spectrum, we estimated the final error for each line flux by means of independent, repeated measurements.

⁵ IRAF is distributed by the National Optical Astronomy Observatories

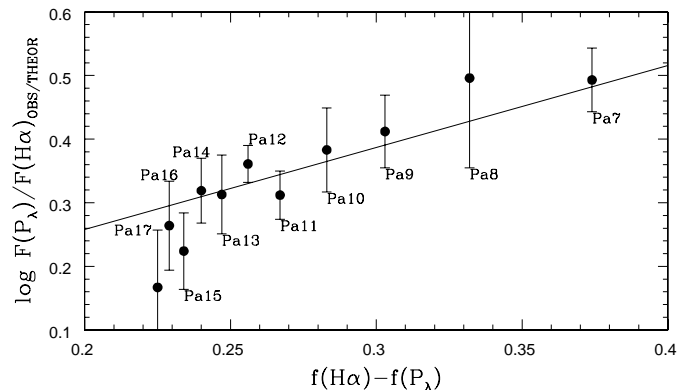


Fig. 2. The ratio between observed and theoretical Paschen to $H\alpha$ flux, $P_\lambda/H\alpha$, versus the reddening function, $f(H\alpha) - f(P_\lambda)$, for IIZw40. The line shows the least-square fit to the data.

We measured, for each galaxy, the main emission lines from the blue to the near-IR: [OII] λ 3727; [OIII] λ 4363; $H\beta$; [OIII] λ 4959,5007; $H\alpha$; [NII] λ 6548,84; [SII] λ 6717,31; [SIII] λ 6312,9069,9532; [ArIII] λ 7136; [OII] λ 7320,30; Pa9 and Pa8, among others. The other Hydrogen Paschen lines series, from Pa13 to Pa8, were detected in some galaxies of our sample. Reddening-corrected line intensity ratios (applying Whitford's 1958 extinction law) normalized to $H\beta=100$ are presented in Table 1, together with the values of the reddening coefficient, $C(H\beta)$, estimated using the $H\alpha/H\beta$ ratio from our blue spectra (Osterbrock 1989). Column (1) lists the common names of the galaxies and, in those cases where the apertures were centered on a secondary knot, there is an indication between brackets for the position of the aperture (see Kehrig et al. 2004 for details). As is well known, IIZw40 presents high extinction (Baldwin et al. 1982). For this galaxy we measured the Paschen series from Pa17 to Pa8, thereby allowing a direct derivation of the reddening coefficient from its red spectrum. In Fig. 2, we illustrate for this galaxy the observed ratio of the fluxes of each Paschen line to $H\alpha$, relative to its theoretical ratio for case B recombination (Storey & Hummer 1995), $[F(P_\lambda)/F(H\alpha)]_{obs}/[F(P_\lambda)/F(H\alpha)]_{theo}$, vs. the reddening function relative to $H\alpha$, $f(H\alpha) - f(P_\lambda)$.

In order to check the reliability of the reduction process, we carried out two tests. Firstly, when the quality of the measurements allowed, we compared the four brightest Paschen lines, normalized to $H\alpha$, with the corresponding predictions for case B recombination (Storey & Hummer 1995). The corrected $P_\lambda/H\alpha$ values are found to be consistent with the theoretical values, within the errors. In the case of Pa8, we notice that the ratios are slightly above the theoretical value. This is mainly due to the fact that the Pa8 and [SIII] λ 9532 Å lines are blended, making the Pa8 flux suffer from some contamination by the [SIII] line. In the second test we compared the ratio of the two near-IR [SIII] lines, $Q[SIII]=[SIII]\lambda$ 9532/ λ 9069 Å, with the theoretical ratio of 2.44 (Mendoza & Zeppen 1982). The values of $Q[SIII]$ are consistent with the theoretical ratio to within the errors, although many galaxies show $Q[SIII]$ values slightly below the theoretical ratio. This effect could be due to two factors: (a) the telluric absorption features were not to

Table 1. Reddening corrected line fluxes, relative to H β =100, and corresponding extinction coefficients for the sample of galaxies.

Galaxy	[OI] 6300	[SIII] 6312	[OI] 6364	[NII] 6548	H α 6563	[NII] 6584	HeI 6678	[SII] 6717	[SII] 6731	HeI 7065	[ArIII] 7136	[OII] 7320	[OII] 7330	Pa12 8750	Pa11 8865	Pa10 9014	Pa9 9229	[SIII] 9069	Pa8 9548	C(H β)
(1)	(2)	(3)	(4)	(5)	(6)	(7)	(8)	(9)	(10)	(11)	(12)	(13)	(14)	(15)	(16)	(17)	(18)	(19)	(20)	(21)
UM238	—	—	—	5.7	286.0	8.6	—	17.2	13.4	5.8	6.8	3.2	1.8	—	—	—	—	3.7	4.7	0.26
UM69(E)	—	—	—	± 1.1	± 5.5	± 1.3	—	± 1.8	± 1.9	± 0.9	± 0.3	± 0.7	± 0.5	—	—	—	—	± 0.5	± 1.0	0.74
UM69(W)	—	—	—	± 1.4	± 2.3	± 1.4	—	± 1.6	± 1.4	—	± 0.9	± 0.7	± 0.6	—	—	—	—	± 1.2	± 0.9	0.74
Tol0104-388	7.1	—	—	± 1.4	± 1.6	± 1.2	—	± 2.2	± 2.0	—	± 0.5	—	—	—	—	—	—	± 1.0	± 0.7	0.18
UM306	± 0.2	—	—	8.3	286.0	22.1	3.3	29.7	21.9	—	9.0	3.6	2.8	—	2.0	1.9	—	48.8 ^a	4.0	0.18
UM307	—	—	—	± 0.5	± 0.6	± 0.2	± 0.3	± 0.3	± 0.1	—	± 0.4	± 0.1	± 0.1	—	± 0.3	± 0.3	—	± 6.5	± 0.9	0.21
Tol0117-414NS(S)	—	—	—	6.1	286.0	16.3	—	23.1	17.9	—	7.0	—	—	—	—	—	—	22.7	3.7	0.25
Tol0117-414NS(N)	—	—	—	± 0.9	± 1.3	± 0.7	—	± 1.3	± 1.2	—	± 0.9	—	—	—	—	—	—	± 6.0	± 2.1	0.10
Tol0117-414NS	—	—	—	15.4	286.0	46.5	4.3	24.0	27.3	—	4.8	2.4	1.5	—	—	2.1	—	18.5	3.7	0.25
Tol0117-414EW(EW)	—	—	—	± 0.5	± 1.0	± 0.7	± 1.0	± 0.7	± 0.6	—	± 0.7	± 0.4	± 0.4	—	—	± 0.7	—	± 1.7	± 0.6	0.31
Tol0117-414EW	12.1	—	—	21.3	286.0	35.6	—	40.3	31.1	—	—	—	—	—	—	—	—	32.5	—	0.10
UM323	± 1.1	—	—	± 1.8	± 2.6	± 1.8	—	± 1.6	± 1.6	—	—	—	—	—	—	—	—	± 12.0	—	0.22
Tol0140-420	16.1	—	—	20.2	286.0	36.9	—	43.0	31.5	—	—	—	—	—	—	—	—	31.7	—	0.10
UM137	± 1.3	—	—	± 2.3	± 6.8	± 1.4	—	± 2.0	± 0.9	—	—	—	—	—	—	—	—	± 12.4	—	0.31
UM151	—	—	—	20.0	286.0	38.1	—	42.9	32.0	—	—	—	—	—	—	—	—	27.9	—	0.88
UM391	—	—	—	± 2.4	± 2.9	± 1.4	—	± 0.5	± 1.1	—	—	—	—	—	—	—	—	± 9.6	—	0.02
UM396	12.1	—	—	17.8	286.0	50.1	—	58.5	43.3	—	—	—	—	—	—	—	—	28.2	—	1.47
UM408	± 1.1	—	—	± 1.0	± 1.9	± 1.2	—	± 1.7	± 2.9	—	—	—	—	—	—	—	—	± 10.5	—	0.41
UM417	16.1	—	—	7.8	286.0	39.2	—	57.8	45.1	—	—	—	—	—	—	—	—	25.9	—	0.53
Tol0226-390	± 1.3	—	—	± 0.3	± 6.6	± 1.0	—	± 1.2	± 1.4	—	—	—	—	—	—	—	—	± 9.0	—	0.35
Tol0306-405	—	—	—	9.9	286.0	17.3	—	26.9	20.1	—	—	—	—	—	—	—	—	9.6	4.8	0.02
Tol0341-407(W)	—	—	—	± 5.1	± 7.4	± 4.7	—	± 6.6	± 5.3	—	—	—	—	—	—	—	—	± 1.3	± 1.2	0.33
Tol0341-407(E)	—	—	—	286.0	12.4	—	—	29.7	20.8	—	—	—	—	—	—	—	—	16.5	—	0.34
Cam0357-3915	—	—	—	± 5.9	± 1.0	—	—	± 2.4	± 2.4	—	—	—	—	—	—	—	—	± 5.4	—	0.33
CTS1006	—	—	—	286.0	18.1	—	—	32.1	28.1	4.8	2.2	—	—	—	—	5.1	—	5.3	4.4	0.34
CTS1008	—	—	—	± 2.8	± 1.8	—	—	± 3.2	± 2.8	± 1.1	± 0.7	—	—	—	—	± 1.0	—	± 1.2	± 1.5	0.47
UM238	—	—	—	13.4	286.0	37.6	—	48.2	33.4	—	7.7	—	—	—	—	1.9	—	28.5	2.8	0.41
UM69(E)	—	—	—	± 2.1	± 3.5	± 2.3	—	± 3.1	± 2.5	—	± 2.7	—	—	—	—	± 0.6	—	± 6.4	± 0.6	0.53
UM69(W)	7.6	—	4.2	26.2	286.0	79.6	—	64.5	25.5	—	5.4	—	—	—	—	—	—	19.5	—	0.35
Tol0104-388	± 2.0	—	± 1.5	± 1.3	± 1.6	± 0.8	—	± 0.8	± 0.7	$\pm 0.$	± 1.2	—	—	—	—	—	—	± 2.9	—	0.35
UM306	—	—	—	7.3	286.0	9.0	3.1	13.4	7.3	3.7	10.2	—	—	—	3.0	6.7	—	27.3	3.9	1.32
UM307	—	—	—	± 1.4	± 1.9	± 1.3	± 0.4	± 0.6	± 0.5	± 0.5	± 0.6	—	—	—	± 0.5	± 1.0	—	± 5.2	± 0.3	0.47
Tol0117-414NS(S)	—	—	—	286.0	6.8	—	—	17.7	11.5	—	6.9	—	—	—	—	—	—	5.5	—	0.34
Tol0117-414NS(N)	—	—	—	± 4.3	± 1.3	—	—	± 1.2	± 1.1	—	± 0.7	—	—	—	—	—	—	± 0.8	—	0.33
Tol0117-414NS	—	—	—	286.0	8.3	—	10.1	8.9	4.5	4.6	—	—	—	—	—	—	—	1.8	—	0.34
Tol0117-414EW(EW)	—	—	—	± 4.1	± 1.3	—	—	± 0.7	± 0.7	± 0.7	± 1.2	—	—	—	—	—	—	± 0.2	—	0.34
Tol0117-414EW	9.8	2.5	4.1	15.8	286.0	31.2	3.3	25.9	21.9	4.2	8.8	3.5	3.0	—	—	—	2.1	20.4	5.5	0.33
UM323	± 0.3	± 0.3	± 0.5	± 0.9	± 1.3	± 1.0	± 0.3	± 0.8	± 0.7	± 0.2	± 0.4	± 0.3	± 0.2	—	—	—	± 0.5	± 3.4	± 2.6	0.06
Tol0140-420	—	—	—	—	286.0	14.1	—	24.3	20.9	—	8.4	—	—	—	—	—	—	7.5	—	0.06
UM137	—	—	—	± 1.6	± 0.9	—	—	± 0.7	± 0.8	—	± 0.1	—	—	—	—	—	—	± 3.5	—	0.06
UM151	—	—	—	1.1	286.0	6.4	4.8	15.5	10.7	2.9	6.2	2.5	2.6	1.6	—	—	3.0	19.1	—	0.06
UM391	± 0.4	—	—	± 0.1	± 4.0	± 0.1	± 0.5	± 0.1	± 0.1	± 0.1	± 0.1	± 0.2	± 0.1	± 0.5	—	—	± 0.6	± 1.7	—	0.06
UM396	—	—	—	—	286.0	16.6	—	37.8	25.3	—	—	4.8	3.8	—	—	—	—	17.5	—	0.15
UM408	—	—	—	± 4.5	± 3.2	—	—	± 3.0	± 2.4	—	—	± 1.2	± 1.0	—	—	—	—	± 2.0	—	0.15
UM417	2.5	—	—	2.4	286.0	6.5	3.3	9.3	6.3	5.2	4.8	1.9	0.9	—	—	2.2	—	11.5	—	0.15
Tol0226-390	± 0.2	—	—	± 0.1	± 5.1	± 0.6	± 0.2	± 0.1	± 0.6	± 0.3	± 0.1	± 0.1	± 0.1	—	—	± 0.5	—	± 2.0	—	0.15
Tol0306-405	—	—	—	4.9	286.0	13.7	3.6	21.3	10.8	3.2	7.2	2.4	1.8	0.9	0.9	1.2	2.3	15.2	5.1	0.24
Tol0341-407(W)	—	—	—	± 0.4	—	± 0.3	± 0.4	± 0.6	± 0.5	± 0.4	± 0.3	± 0.2	± 0.2	± 0.2	± 0.1	± 0.2	± 0.5	± 1.3	± 0.6	0.24
Tol0341-407(E)	3.2	1.6	—	5.1	286.0	13.4	3.9	16.7	13.7	3.7	9.5	3.2	1.6	—	—	—	4.2	17.4	4.7	0.24
Cam0357-3915	± 0.1	± 0.4	—	± 0.3	± 0.5	± 0.3	± 0.3	± 0.4	± 0.4	± 0.3	± 0.6	± 0.5	± 0.3	—	—	—	± 1.0	± 3.3	± 1.4	0.24

Table 1. continued.

Galaxy	[OI] 6300	[SIII] 6312	[OI] 6364	[NII] 6548	H α 6563	[NII] 6584	HeI 6678	[SII] 6717	[SII] 6731	HeI 7065	[ArIII] 7136	[OII] 7320	[OII] 7330	Pa12 8750	Pa11 8865	Pa10 9014	Pa9 9229	[SIII] 9069	Pa8 9548	C(H β)
(1)	(2)	(3)	(4)	(5)	(6)	(7)	(8)	(9)	(10)	(11)	(12)	(13)	(14)	(15)	(16)	(17)	(18)	(19)	(20)	(21)
Tol0528-383(E)	—	—	—	10.3 ± 2.9	286.0 ± 3.2	18.0 ± 2.9	—	39.9 ± 2.1	30.4 ± 2.7	—	11.3 ± 1.9	—	—	—	—	—	—	19.9 ± 3.0	3.9 ± 1.3	0.46
Tol0528-383(W)	—	—	—	10.2 ± 1.9	286.0 ± 2.0	16.4 ± 1.8	—	31.6 ± 1.8	22.0 ± 1.4	—	9.2 ± 1.6	—	—	—	—	—	2.7 ± 0.9	13.5 ± 2.5	5.0 ± 1.5	0.46
Tol0538-416	4.5 ± 0.4	2.0 ± 0.3	3.0 ± 0.4	5.1 ± 0.7	286.0 ± 0.9	14.9 ± 0.6	4.0 ± 0.4	24.4 ± 0.8	15.9 ± 0.6	3.4 ± 0.5	16.7 ± 0.5	—	—	—	2.3 ± 0.6	—	—	19.2 ± 4.1	4.7 ± 2.9	0.14
IIZw40	1.8 ± 0.2	1.1 ± 0.2	—	—	286.0 ± 0.3	6.4 ± 0.2	3.5 ± 0.3	7.6 ± 0.4	6.2 ± 0.3	4.6 ± 0.2	8.3 ± 0.3	1.4 ± 0.2	1.1 ± 0.2	1.1 ± 0.1	1.3 ± 0.1	1.9 ± 0.3	2.7 ± 0.3	15.3 ± 1.6	4.3 ± 1.4	1.29
Cam0840+1201	4.4 ± 0.4	2.2 ± 0.3	—	5.2 ± 0.2	286.0 ± 0.2	12.5 ± 0.2	—	21.9 ± 0.3	16.0 ± 0.3	3.4 ± 0.2	7.1 ± 0.3	3.2 ± 0.2	2.7 ± 0.2	1.1 ± 0.7	—	1.8 ± 0.2	—	16.2 ± 5.1	7.3 ± 1.3	0.02
Tol1924-416	4.9 ± 0.2	1.5 ± 0.2	1.1 ± 0.2	3.5 ± 0.2	286.0 ± 0.6	8.9 ± 0.3	3.5 ± 0.1	14.7 ± 0.1	11.4 ± 0.1	2.9 ± 0.1	5.2 ± 0.1	2.4 ± 0.2	2.0 ± 0.1	—	1.4 ± 0.2	1.8 ± 0.3	—	11.7 ± 1.4	4.3 ± 0.7	0.10
Tol2019-405(NE)	—	—	—	7.4 ± 1.3	286.0 ± 2.0	14.9 ± 1.5	—	30.1 ± 2.8	24.3 ± 2.8	—	6.1 ± 1.2	3.2 ± 0.9	2.8 ± 1.0	—	—	—	—	29.4 ± 4.6	8.7 ± 2.5	0.10
Tol2019-405	—	—	—	7.7 ± 1.6	286.0 ± 2.6	17.4 ± 1.9	—	36.0 ± 2.3	29.9 ± 2.7	—	6.9 ± 1.6	—	—	—	—	—	—	30.2 ± 6.4	8.3 ± 1.9	0.10
Tol2138-397	—	—	—	—	286.0 ± 7.4	—	—	14.8 ± 0.8	7.5 ± 0.5	—	—	5.4 ± 0.4	—	—	—	—	—	14.7 ± 2.8	—	0.11
Tol2146-391	23.2 ± 1.0	—	—	3.4 ± 0.2	286.0 ± 188.6	5.5 ± 0.3	—	11.0 ± 0.8	7.5 ± 0.5	4.5 ± 0.2	8.5 ± 0.5	2.9 ± 0.1	2.6 ± 0.1	—	1.5 ± 0.3	2.4 ± 0.4	—	28.2 ^a ± 2.7	—	0.12
MCG-05-52-065(E)	—	—	—	25.5 ± 2.8	286.0 ± 4.1	59.1 ± 2.9	5.6 ± 1.9	67.4 ± 2.8	46.5 ± 2.2	—	8.4 ± 1.3	—	—	—	—	—	—	31.3 ± 3.6	4.6 ± 1.4	0.44
MCG-05-52-065(W)	—	—	—	24.1 ± 4.5	286.0 ± 8.4	89.4 ± 6.7	—	88.8 ± 8.7	69.8 ± 6.6	—	—	—	—	—	—	—	—	29.5 ± 4.5	—	0.44
Tol2240-384	2.9 ± 0.6	—	—	—	286.0 ± 0.3	3.8 ± 0.3	2.1 ± 0.4	6.8 ± 0.3	5.6 ± 0.3	—	4.4 ± 0.1	—	—	—	—	—	2.8 ± 1.7	8.6 ± 3.2	—	0.36
UM160(E)	—	—	—	3.2 ± 0.2	286.0 ± 3.6	10.0 ± 0.9	4.8 ± 1.6	24.8 ± 1.6	17.1 ± 0.5	—	5.1 ± 0.4	—	—	—	—	—	—	13.6 ± 2.7	—	0.26
UM160(W)	—	—	—	—	286.0 ± 1.6	13.4 ± 1.6	—	38.6 ± 0.8	27.2 ± 1.4	—	—	—	—	—	—	—	—	23.6 ± 4.9	—	0.26
UM166	—	—	—	17.4 ± 1.6	286.0 ± 2.8	58.3 ± 1.7	—	34.4 ± 2.3	31.7 ± 2.0	—	6.2 ± 1.3	—	—	—	—	—	—	54.1 ^a ± 5.8	—	0.25
UM167	5.9 ± 0.3	—	1.4 ± 0.1	36.6 ± 1.1	286.0 ± 2.1	105.6 ± 0.6	2.5 ± 0.3	30.2 ± 0.5	29.8 ± 0.7	2.8 ± 0.3	4.0 ± 0.1	3.0 ± 0.2	2.4 ± 0.1	0.8 ± 0.1	0.9 ± 0.2	1.2 ± 0.2	2.3 ± 0.6	24.1 ± 2.8	4.1 ± 0.9	0.30

^a We have quoted the flux of [SIII] λ 9532 Å instead of [SIII] λ 9069 Å

tally removed and/or (b) the [SIII] λ 9532 Å line flux could be blended with the Pa8 line.

These two tests lead us to conclude that the correction for atmospheric absorption, though not perfect, has provided generally satisfactory results for the purposes of this study.

3. Results and Discussion

3.1. Empirical abundance indicators for our sample

Commonly used strong line empirical abundance indicators are R_{23} (Pagel et al. 1979; Edmunds & Pagel 1984; McCall et al. 1985; McGaugh 1991) and $S_{23(4)}$ (Vílchez & Esteban 1996; Díaz & Pérez-Montero 2000; Oey & Shields 2000; PM06). Though widely used, R_{23} presents the drawback of having a double-valued relation with oxygen abundance, creating an intrinsic uncertainty on the derived O/H abundances. The turnover region of the relation R_{23} vs. O/H takes place for $\log R_{23} \gtrsim 0.9$, corresponding to $8.0 \lesssim 12+\log(O/H) \lesssim 8.4$. In this region, R_{23} is sensitive to ionization conditions but almost insensitive to O/H. Most of the HII galaxies from our sample show R_{23} values within this ill-defined region, which is what we want to explore.

The S_{23} parameter introduced by Vílchez & Esteban (1996) has been used as an O/H abundance calibrator in Díaz & Pérez-Montero (2000) and Pérez-Montero & Díaz 2005 (hereinafter PMD05). It has also been demonstrated that S_{23} is an efficient S/H abundance calibrator in PM06. It presents several advantages over R_{23} . First, it has a lower dependence on the ionization parameter and remains single-valued up to metallicities higher than solar, $12+\log(O/H)_{\odot} = 8.69$ and $12+\log(S/H)_{\odot} = 7.19$ (Lodders 2003). Secondly, the sulfur emission lines are less affected by reddening. However, the spectral regions around the red [SIII] lines are affected by atmospheric absorption.

The $N2^6$ parameter has also been proposed as an abundance indicator (Denicoló et al. 2002; Van Zee et al. 1998). This parameter offers several advantages, because it involves easily measurable lines that are available for a wide redshift range (up to $z \sim 2.5$). The $N2$ vs. O/H relation seems monotonic and the [NII]/ $H\alpha$ ratio does not depend on reddening correction or flux calibration. The drawbacks are that the [NII] lines can be affected by other excitation sources (see Van Zee et al. 1998). In addition, $N2$ is sensitive to ionization conditions and relative N/O abundance variations.

Figure 3a shows the relation between S_{23}^7 and R_{23}^8 for the galaxies of our sample. Although $\log R_{23}$ values remain approximately constant for most galaxies, $\log S_{23}$ values present a variation of approximately 0.8 dex. We can see that for galaxies in the turn-over region of the relation between R_{23} and O/H, R_{23} does not correlate with S_{23} . This fact is easily understood since the relationship between S_{23} and O/H is not bivariate in the metallicity range that we are interested in. Besides, Figs. 3b

and c show that R_{23} does not correlate with [NII]/ $H\alpha$, contrary to the behavior of S_{23} . Therefore, for objects located in the ill-defined region of R_{23} vs. O/H, S_{23} can be used to derive chemical abundances, especially the S/H abundance.

3.2. Ionization structure and the ionizing sources

In photoionized regions like the ones we consider here, the physical properties that determine line intensities are the luminosities and temperatures of the ionizing stars, the gas density, the optical thickness to the ionizing photons, and the chemical abundances. Because S_{23} is a combination of strong line intensities, it can be affected by several effects. Taking S_{23} as an abundance indicator, we are not considering, to first order, the detailed effects produced by changes in the physical properties mentioned above. For this reason, it is important to check the sensitivity of S_{23} to some of these properties.

The optical thickness to ionizing photons is the first to assess. As can be seen in Fig. 4a, [NII]/ $H\alpha$ and [SII]/ $H\alpha$ present a strong correlation, discarding density boundary effects for the sample galaxies (see e.g. McCall et al. 1985); this correlation implies a statistically significant relation between N^+/N and S^+/S , as expected from standard HII region models.

Ratios of line intensities of elements in different ionization stages, such as [OIII]/[OII] or [SIII]/[SII], are sensitive to combinations of the luminosity, the gas density and geometry, and the radiation hardness; but they are insensitive to abundances at first order, as they originate in the same element. Any variation with respect to such line ratios indicates a sensitivity to these physical parameters, though in a combination that might not be straightforward to derive.

Figure 4b shows the dependence of S_{23} on [SIII]/[SII]⁹. While [NII]/ $H\alpha$ shows a well-known dependence on the excitation degree (e.g. McCall et al. 1985), the dependence is much weaker for S_{23} , being mostly marginal. Despite the fact that S_{23} possesses a narrower dynamical range than [NII]/ $H\alpha$, we consider it a better abundance indicator for our sample than [NII]/ $H\alpha$, since S_{23} does not show any strong dependence on the ionization conditions.

Having a wide wavelength coverage has allowed us to study the properties of the ionizing sources in our sample of HII galaxies. This study could help to constrain the range of applicability of photoionization models and stellar atmospheres in order to fit the observations, thus improving our understanding of the mechanisms that heat the HII regions in HII galaxies (Stasińska & Schaerer 1999; Thuan & Izotov 2005). A convenient hardness index is the parameter η' introduced by Vílchez & Pagel (1988):

$$\eta' = \frac{[OII]\lambda\lambda 3727, 29/[OIII]\lambda\lambda 4959, 5007}{[SII]\lambda\lambda 6717, 31/[SIII]\lambda\lambda 9069, 9532}$$

This parameter has been recommended as a criterion for effective temperature of the ionizing star(s), T_{eff} , of HII regions, in the sense that softer ionizing spectra have higher values of η' (e.g. Vílchez & Pagel 1988; Kennicutt et al. 2000). In Fig. 5a we present the behavior of the parameter η' with respect to

⁶ $N2 = \log([NII]\lambda 6584/H\alpha)$

⁷ The S_{23} values were derived using the sulfur emission lines quoted in Table 1

⁸ The R_{23} values were calculated using the oxygen emission lines from our blue spectra (Kehrig et al 2004).

⁹ $[SIII]/[SII] = [SIII]\lambda\lambda 9069, 9532/[SII]\lambda\lambda 6717, 6731$

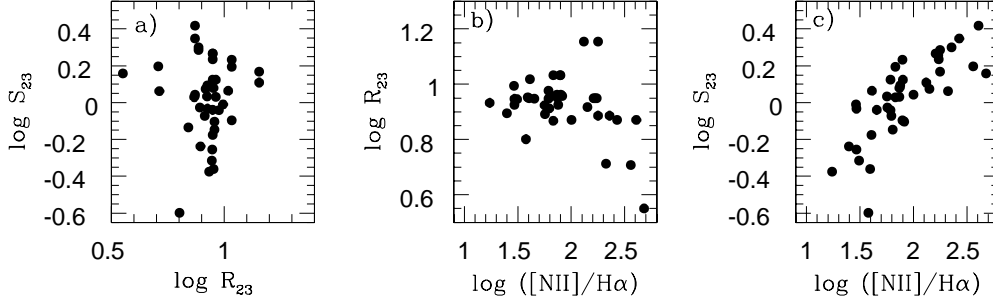


Fig. 3. The left panel presents the relation between S_{23} and R_{23} ; the middle and right panels show the relations between $\log (1.3x[\text{NII}]6584/H\alpha)$ and the empirical indicators of abundances, R_{23} and S_{23} respectively, for all galaxies of our sample.

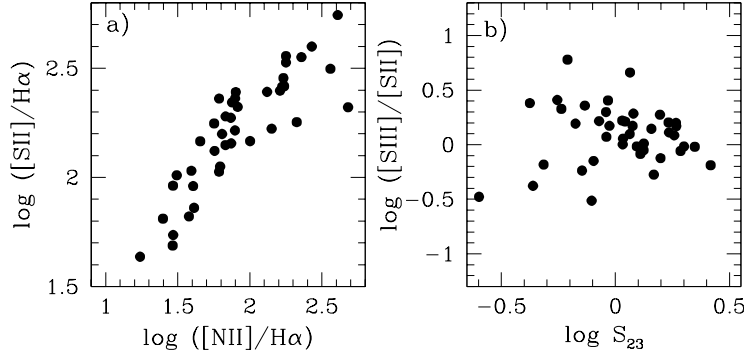


Fig. 4. The left panel shows the relation of $\log ([\text{SII}]6717,31/H\alpha)$ vs. $\log (1.3x[\text{NII}]6584/H\alpha)$; the right panel presents the relation between $\log ([\text{SIII}]/[\text{SII}])$ and $\log S_{23}$ for all galaxies of our sample.

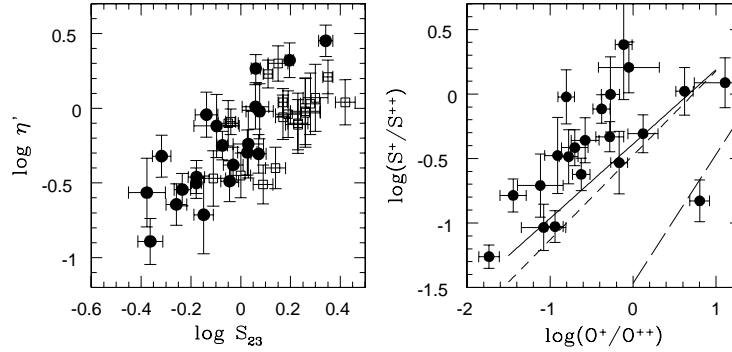


Fig. 5. The left panel shows the relation $\log \eta'$ vs. $\log S_{23}$ for all galaxies in our sample. Full and empty symbols represent the objects with and without $T_e[\text{OIII}]$, respectively. The right panel presents the relation between $\log (S^+/S^{++})$ and $\log (O^+/O^{++})$ for the galaxies with electron temperature; solid, short-dashed, and long-dashed lines show the loci for three series of photoionization models for $T_{eff}=50\text{kK}$, 40kK , and 30kK , respectively. See the text for details.

S_{23} for our sample. Overall, we can see that η' goes up with S_{23} , implying that the hardness of the ionizing spectra increases with lower gaseous metallicity for our sample of HII galaxies (e.g. Bresolin & Kennicutt 1999; Oey et al. 2000 and references therein; see also Martín-Hernández et al. 2002). A possible explanation for higher temperatures at lower metallicities has been suggested by Massey et al. (2004). They find that, for a range of stellar atmosphere models, stars of early through mid-O types in a Magellanic Cloud sample are 3000K-4000K hotter than their Galactic (metal-rich) counterparts; and they

attribute their higher temperatures to the minor importance of wind emission, wind blanketing, and metal-line blanketing at lower metallicities.

In Fig. 5b we present the relationship between the ionic ratios S^+/S^{++} and O^+/O^{++} for the subset of HII galaxies with electron temperature. In this figure we show the loci of the average predictions of three sequences of single-star photoionization models (computed with the photoionization code Cloudy 96; Ferland 2002), performed using CoStar model atmospheres (Schaerer & de Koter 1997) $T_{eff}=50\text{kK}$, 40kK and 30kK .

Along each line, the metallicities vary between $Z_{\odot}/20$ and $Z_{\odot}/2$, and the ionization parameter changes from $\log U = -2$ to $\log U = -3$ (a detailed description of the grids of the photoionization models used in this work can be found in PMD05). According to these models, a large fraction of the galaxies appear to harbor ionizing sources with spectra harder than the spectrum produced by a 50kK effective temperature CoStar atmosphere (Schaerer & de Koter 1997). Kennicutt et al. (2000) have found, for a sample of HII regions (in the Galaxy and Magellanic Cloud), that empirically-based stellar-temperature indices present a decrease in mean stellar temperature with increasing abundance. They show, however, that the typical T_{eff} for their HII regions are below $\sim 55\text{kK}$ (at $Z_{\odot}/5$), in agreement with the model-based results by Bresolin et al. (1999). Though any calibration of nebular empirical parameters in terms of T_{eff} should be a function of the atmosphere and photoionization models used, it seems that $T_{eff} \sim 55\text{kK}$ represents a reasonable upper limit for the effective temperature in HII regions in contrast to HII galaxies. These findings suggest the existence of very hard spectral energy distributions as ionizing sources in some HII galaxies. Stasińska & Schaerer (1999), modelling the HII regions in IZw18, argue that extra heating sources might well exist, in addition to ionizing clusters, giving rise to large temperature variations and enhancing the [OIII] $\lambda 4363$ emission. I05 have also invoked extra heating sources (i.e. X-ray ionizing sources) to explain the high-ionization emission lines observed in some metal-poor emission-line galaxies. More observations, covering a wide range in wavelength, as well as dedicated work using photoionization models for evolving starbursts with a library of different ionizing spectra, are needed to further investigate the above suggestions.

3.3. Physical properties and chemical abundances

The physical properties and chemical abundances of the ionized gas were calculated for these galaxies following the 5-level atom FIVEL program (Shaw & Dufour 1994) available in the task IONIC of the STSDAS package. The final quoted errors in the derived quantities were calculated by error propagation including errors in flux measurements, atmospheric corrections, and temperatures. For the [SIII] lines we adopted the most recent atomic coefficients (Tayal & Gupta 1999).

Electron densities were obtained from the [SII] $\lambda 6717/\lambda 6731$ Å line ratio. We could derive the electron temperature values of $T_e[\text{SIII}]$, $T_e[\text{OIII}]$, $T_e[\text{OII}]$, and $T_e[\text{SII}]$ by combining the data from our blue (Kehrig et al. 2004) and red spectra. Using the [OIII] $\lambda 4363/\lambda 4959, 5007$ Å line ratio, we derived the $T_e[\text{OIII}]$ for 21 galaxies of the sample. The $T_e[\text{SIII}]$ was calculated from the [SIII] $\lambda 6312/\lambda 9069, 9532$ Å line ratio for 14 galaxies with a measurement of the [SIII] $\lambda 6312$ Å line. For the 8 galaxies without any measurement of the [SIII] $\lambda 6312$ Å line and with $T_e[\text{OIII}]$, a theoretical relation between [OIII] and [SIII] electron temperatures (PMD05) was used:

$$T_e[\text{SIII}] = 10,500 T_e[\text{OIII}] - 800$$

In total we have 22 galaxies with a measurement of $T_e[\text{SIII}]$. In order to derive $T_e[\text{SIII}]$ temperature and S^{++} abundances,

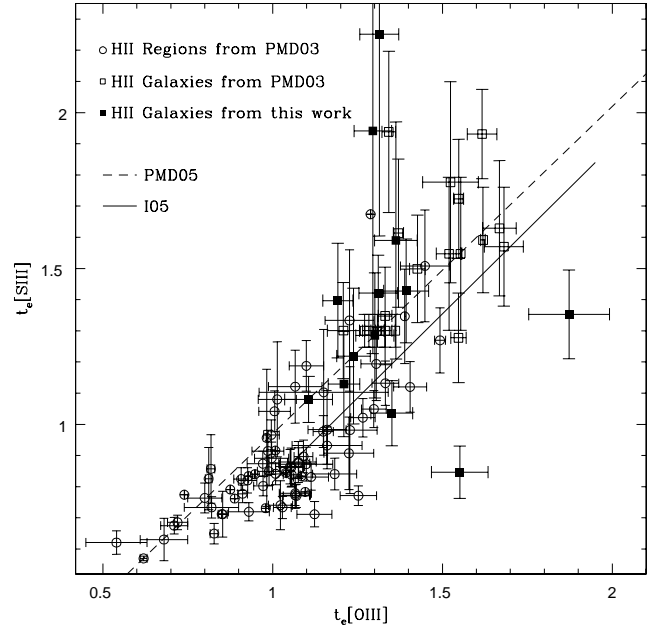


Fig. 6. A comparison between the measured line temperatures of [OIII] and [SIII]. The electron temperatures, $T_e[\text{OIII}]$ and $T_e[\text{SIII}]$, are shown in units of 10^4K . The dashed and solid lines are the photoionization models' relation between these temperatures from PMD05 and I05, respectively.

whenever possible we used the [SIII] $\lambda 9069$ Å fluxes, given that the flux of [SIII] $\lambda 9532$ Å seems to be affected by partial blending of the P8 line. However, when the [SIII] $\lambda 9069$ Å line falls inside the absorption band head due to the redshift of the galaxy, the flux of the [SIII] $\lambda 9532$ Å line was used if this line was not close to the $1\mu\text{m}$ limit, where the flux calibration becomes highly uncertain.

Regarding [SII] temperatures, for those objects without the [SII] auroral line at $\lambda 4068$ Å we took the approximation $T_e[\text{SII}] \approx T_e[\text{OII}]$ as valid. We could derive $T_e[\text{OII}]$ using the [OII] $\lambda 3727/7325$ Å line ratio for 16 objects of the sample. For the rest of the objects not presenting any auroral line in the low excitation zone, we used the model-predicted relations between $T_e[\text{OII}]$ and $T_e[\text{OIII}]$ found in PMD03, which explicitly take the dependence of $T_e[\text{OII}]$ on electron density into account. In most cases the agreement between our line-intensity measurements in the blue and in the red spectra is good; we thus have adopted the values with the smaller observational errors to derive line temperatures. Otherwise, for $T_e[\text{SIII}]$ and $T_e[\text{SII}]$, we used the line intensities corresponding to the red spectra.

The relationship between both temperatures, $T_e[\text{OIII}]$ and $T_e[\text{SIII}]$, is shown in Fig. 6 for all our galaxies with electron temperature and the sample of HII galaxies and HII regions compiled in PMD03, together with photoionization model relations. We note that there are two behaviors. While most HII regions show lower $T_e[\text{SIII}]$ values than the ones provided by the photoionization models relations, many HII galaxies present higher $T_e[\text{SIII}]$ values than the ones predicted by the models. The same trend can be noticed for the sample of metal-

Table 2. Physical properties and chemical abundances for the galaxies with S/H and O/H derived directly

Object	G89 ^a	IIZW40 PMD03 ^a	This Work	Tol0226-390	Tol1924-416	Tol0538-416
n_e ([SII])	100.	290±60	197±167	221 ±64	78±28	≤ 100. ^b
T_e ([SIII])/10 ⁴ K	1.35±0.12	1.30±0.05	1.04 ^c ±0.10	1.40 ^c ±0.18	1.43 ^c ±0.17	1.29 ^c ±0.20
T_e ([OIII])/10 ⁴ K	1.33±0.02	1.34±0.03	1.35±0.06	1.19±0.04	1.39±0.07	1.30±0.06
12+log(S ⁺ /H ⁺)	5.21 ±0.09	5.21±0.09	5.23±0.12	5.81±0.07	5.50±0.06	6.18±0.04
12+log(S ⁺⁺ /H ⁺)	6.00 ±0.11	5.99±0.04	6.24±0.14	6.17±0.16	5.91±0.13	6.20±0.21
12+log[(S ⁺ + S ⁺⁺)/H ⁺]	6.07±0.11	6.07±0.05	6.28±0.14	6.33±0.13	6.06±0.11	6.49±0.13
ICF(S ⁺ + S ⁺⁺)	1.95	1.86	1.98	1.05	1.06	1.06
12+log (S/H)	6.36±0.11	6.34±0.05	6.53±0.34	6.35±0.14	6.08±0.12	6.53±0.14
12+log(O ⁺ /H ⁺)	6.95±0.07	7.08±0.07	6.88±0.26	7.37±0.15	7.13±0.14	6.99±0.07
12+log(O ⁺⁺ /H ⁺)	8.01±0.02	8.03±0.08	7.96±0.07	7.94±0.07	7.83±0.08	7.79±0.07
12+log (O/H)	8.05±0.02	8.08±0.03	7.99±0.09	8.05±0.09	7.91±0.09	7.86±0.07
Object	Cam0840+1201	CTS1008	UM238	Tol0104+388	UM306	UM307
n_e ([SII])	≤ 100. ^b	169±50	≤ 100. ^b	≤ 100. ^b	111±109	845±102
T_e ([SIII])/10 ⁴ K	1.59 ^c ±0.38	1.22 ^c ±0.22	1.61 ^d ±0.09	0.85 ^e ±0.08	1.13 ^e ±0.17	1.08 ^e ±0.07
T_e ([OIII])/10 ⁴ K	1.36±0.06	1.24±0.05	1.61±0.09	1.55±0.08	1.21±0.05	1.11±0.07
12+log(S ⁺ /H ⁺)	5.52±0.05	5.50±0.11	5.54±0.17	6.13±0.03	5.83±0.05	6.40±0.17
12+log(S ⁺⁺ /H ⁺)	6.00±0.29	6.20±0.22	5.34±0.09	6.96±0.16	6.36±0.24	6.31±0.10
12+log[(S ⁺ + S ⁺⁺)/H ⁺]	6.12±0.24	6.28±0.20	5.75±0.14	7.02±0.14	6.48±0.20	6.66±0.14
ICF(S ⁺ + S ⁺⁺)	1.74	1.09	1.01	1.00	1.09	1.04
12+log (S/H)	6.36±0.33	6.32±0.22	5.76±0.14	7.02±0.18	6.52±0.21	6.68±0.14
12+log(O ⁺ /H ⁺)	6.86±0.14	6.90±0.27	7.60±0.36	8.33±0.09	7.75±0.07	8.68±0.35
12+log(O ⁺⁺ /H ⁺)	7.77±0.07	8.01±0.07	7.65±0.08	7.53±0.08	7.92±0.07	7.57±0.11
12+log (O/H)	7.82±0.08	8.05±0.09	7.92±0.23	8.40±0.09	8.14±0.07	8.71±0.34
Object	UM323	Tol0140+420	UM391	UM396	UM408	Tol0306+405
n_e ([SII])	630: ^f	144: ^f	≤ 100. ^b	≤ 100. ^b	≤ 100. ^b	220±64
T_e ([SIII])/10 ⁴ K	1.35 ^e ±0.14	2.25 ^e ±0.65	1.09 ^e ±0.10	1.31 ^d ±0.06	1.71 ^d ±0.11	1.94 ^e ±0.71
T_e ([OIII])/10 ⁴ K	1.87±0.12	1.31±0.06	1.12±0.09	1.32±0.06	1.71±0.10	1.29±0.06
12+log(S ⁺ /H ⁺)	5.88±0.13	5.83±0.07	6.02±0.05	5.30±0.04	5.36±0.05	5.94±0.04
12+log(S ⁺⁺ /H ⁺)	5.86±0.13	5.83±0.28	6.33±0.14	6.33±0.12	5.47±0.10	5.56±0.43
12+log[(S ⁺ + S ⁺⁺)/H ⁺]	6.17±0.13	6.13±0.19	6.50±0.11	6.37±0.11	5.72±0.08	6.09±0.19
ICF(S ⁺ + S ⁺⁺)	1.02	1.03	1.02	1.78	1.01	1.01
12+log (S/H)	6.18±0.13	6.16±0.18	6.51±0.11	6.61±0.17	5.73±0.08	6.13±0.16
12+log(O ⁺ /H ⁺)	7.99±0.07	7.51±0.08	7.49±0.12	7.03±0.07	7.18±0.07	7.78±0.07
12+log(O ⁺⁺ /H ⁺)	7.37±0.08	7.78±0.07	7.37±0.14	7.97±0.07	7.56±0.08	7.90±0.07
12+log (O/H)	8.08±0.07	7.96±0.08	7.74±0.13	8.01±0.07	7.71±0.08	8.15±0.07
Object	Cam0357+3915	CTS1006	Tol2138+397	Tol2146+391	Tol2240+384	UM151 ^g
n_e ([SII])	≤ 100. ^b	≤ 100. ^b	≤ 100. ^b	≤ 100. ^b	132±80	≤ 100. ^b
T_e ([SIII])/10 ⁴ K	1.52 ^d ±0.08	1.42 ^e ±0.12	1.99 ^d ±0.14	1.68 ^d ±0.10	1.60 ^d ±0.09	1.88 ^d ±0.12
T_e ([OIII])/10 ⁴ K	1.52±0.08	1.31±0.06	1.97±0.13	1.68±0.10	1.60±0.09	1.86±0.12
12+log(S ⁺ /H ⁺)	5.07±0.07	5.70±0.07	5.20±0.04	4.93±0.05	5.19±0.05	5.77±0.06
12+log(S ⁺⁺ /H ⁺)	5.86±0.11	6.03±0.09	5.82±0.12	6.20±0.08	5.68±0.20	6.13±0.13
12+log[(S ⁺ + S ⁺⁺)/H ⁺]	5.93±0.10	6.20±0.09	5.91±0.10	6.22±0.07	5.80±0.17	6.29±0.11
ICF(S ⁺ + S ⁺⁺)	1.14	1.06	1.12	1.10	1.14	1.04
12+log (S/H)	5.98±0.13	6.22±0.09	5.96±0.12	6.26±0.09	5.86±0.20	6.31±0.12
12+log(O ⁺ /H ⁺)	6.33±0.14	7.54±0.15	6.69±0.07	5.88±0.10	6.92±0.08	—
12+log(O ⁺⁺ /H ⁺)	7.78±0.08	7.82±0.07	7.31±0.08	7.61±0.08	7.70±0.08	7.05 ±0.08
12+log (O/H)	7.79±0.08	8.00±0.10	7.41±0.08	7.62±0.08	7.77±0.08	—

^a References - G89: Garnett (1989), PMD03: Pérez-Montero & Díaz (2003)^b Low Density Limit^c T_e ([SIII]) derived using [SIII]λ6312 Å line from the red spectra^d T_e ([SIII]) derived from the relation T_e ([SIII]) = 10500 T_e ([OIII]) - 800, see the text for details.^e T_e ([SIII]) derived using [SIII]λ6312 Å line from the blue spectra^f Upper limit^g [OII]λ3727 Å line could not be measured for UM151

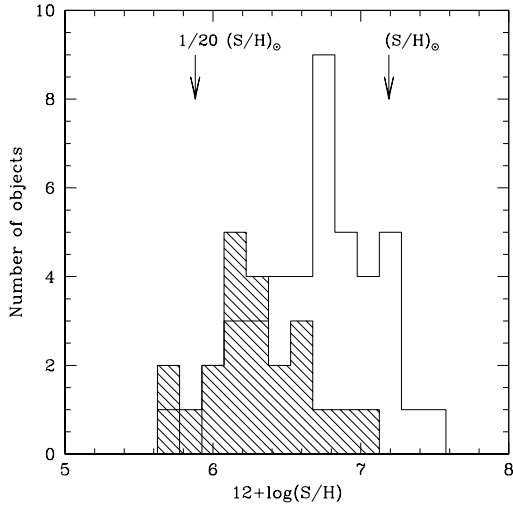


Fig. 7. The distribution of total sulfur abundance for our sample of galaxies. The dashed and empty histograms show the number of galaxies with S/H derived from $T_e[\text{SIII}]$ (see Table 2) and obtained from the S_{23} calibration, respectively (see the text for details).

poor emission-line galaxies in I05 (their Fig.4), for a range of $T_e[\text{OIII}]$ from $1 \times 10^4 \text{ K}$ to $2.0 \times 10^4 \text{ K}$. This fact suggests that HII regions and HII galaxies probably present different spatial temperature structures.

In order to compute the total sulfur abundances, we need to evaluate the corresponding ICF. A detailed study of the ICF scheme for sulfur is described in PM06. According to this work, for the objects with $\log([\text{SIII}]/[\text{SII}]) \geq 0.4$, we made use of the formula of Barker with $\alpha = 2.5$ (Barker 1980). For the rest of the objects in the sample, we used the predictions of photoionization models for CoStar atmospheres (see Fig.3 in PM06). These predictions indicate rather low values of the ICF, independent of the ionizing effective temperature of the models.

With regard to the oxygen ICF, a small fraction of O/H is expected to be in the form of O^{3+} ion in the high-excitation HII regions when the $\text{HeII}\lambda 4686$ emission line is detected. We have a measurement of the $\text{HeII}\lambda 4686$ emission line in 6 galaxies of our sample. According to the photoionization models from Stasińska & Izotov (2003), the O^{3+}/O can be on the order of 1% only in the highest-excitation HII regions [$\text{O}^{3+}/(\text{O}^{3+} + \text{O}^{2+}) \leq 0.1$]; therefore, taking our abundance results into account, we assumed that this correction is negligible in our sample.

Physical conditions, chemical abundances, and ICFs of sulfur for the galaxies with a measurement of the $T_e[\text{SIII}]$ are quoted in Table 2. From this Table we can see that there are six galaxies with $12+\log(\text{O}/\text{H})$ varying between 7.4 and 7.8. These objects are among the galaxies with very low metallicity. For the objects without $T_e[\text{SIII}]$, we used the strong line calibration of the total S/H abundance as a function of S_{23} , presented by PM06, to derive the total S/H abundance.

The only galaxy of our sample for which we can compare the S/H abundance derived in this work with previous S/H abundance determinations in the literature is IIZw40. This galaxy has been observed by G89 and PMD03. In Table 2 we

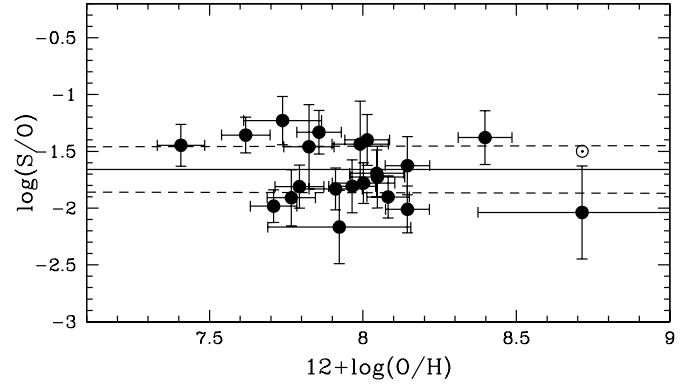


Fig. 8. The observed sulfur-to-oxygen abundance ratio for the subset of galaxies of the sample with $T_e[\text{OIII}]$ plotted as a function of the oxygen abundance. The solar value is shown. The dashed lines are $\pm 1\sigma$ of the mean as shown by the continuous line.

present the results for IIZw40 obtained by the three works. In order to minimize possible reddening corrections effects in the abundance calculation for this galaxy, we referred the flux of each sulfur line we measured to a nearby hydrogen line. In the case of $12+\log(\text{S}^+/\text{H}^+)$ ionic abundance the three values are close to each other; the value of the $12+\log(\text{S}^{++}/\text{H}^+)$ ionic abundance, derived in this work is higher than the previous ones by up to some 0.2 dex. We believe that this fact could be the result of our systematic absorption correction procedure.

Figure 7 shows the distribution of sulfur abundance derived for our sample of HII galaxies. The empty and dashed histograms represent the distribution of S/H derived with S_{23} for all the objects and obtained from $T_e[\text{SIII}]$, respectively. Most of the galaxies present total S/H abundance values that are between $1/20$ solar to solar¹⁰. This is an expected behavior since our sample is composed mainly of low-luminosity galaxies. Besides, we note that the dashed histogram peak corresponds to total S/H abundance value lower than the S/H maximum of the empty histogram. It suggests that, in order to know the overall metallicity distribution of a sample of galaxies, it would be worth making use of an efficient empirical abundance indicator. Hoyos & Díaz (2006) found a similar result by studying the O/H abundance for a sample of HII galaxies.

The abundances obtained in this work allow us to study the dependence of S/H as a function of O/H in low metallicity environments. In Fig. 8 we show the relationship between the S/O abundance ratio and total O/H abundance for the subset of galaxies with $T_e[\text{OIII}]$ and $T_e[\text{SIII}]$. The value of the sigma weighted mean for $\log(\text{S}/\text{O})$ is -1.68 ± 0.20 dex. The galaxy with nearly solar metallicity (UM307) is classified as an SABd from HYPERLEDA database¹¹.

Evaluating the contribution of all observational errors to the derivation of these abundances, we can conclude at this level of uncertainty that there is no statistical evidence of any systematic variation of S/O with O/H for this range of abundances. Therefore, our results agree with a constant S/O ratio and lower (1σ) than the solar ratio for this type of emission-

¹⁰ $12+\log(\text{S}/\text{H})_{\odot} = 7.19 \pm 0.04$ (Lodders 2003)

¹¹ leda.univ-lyon1.fr (Paturel 2003)

line object. This result indicates that sulfur and oxygen appear to be produced by the same massive stars, as expected by current nucleosynthesis prescriptions (see Pagel 1997 and references therein). In recent works, I05 and PM06 indicate that HII galaxy data are consistent with a constant S/O ratio, but somewhat lower than the current solar ratio. Regarding disk HII regions, the dispersion in S/O appears much larger and the assumptions of a constant S/O is questionable there. These results suggest that the assumption that the S/O ratio is constant at all abundances remains controversial (e.g. Bresolin et al. 2004) and should be explored further, particularly at the not very well-known metallicity ends: extremely metal deficient HII galaxies (i.e. very low O/H) and HII regions in the inner disk of galaxies (i.e. metal rich central parts with highest O/H).

4. Summary

In this work we have performed a long-slit spectroscopic study of a sample of 34 HII galaxies observed in the blue and near-IR ranges (3700Å-1μm). The red spectra were carefully corrected for the effects of the telluric atmospheric absorption. Measurements of the nebular [SIII] lines at $\lambda\lambda 9069, 9532$ were obtained for all objects.

Whenever possible we derived values of T_e [SIII], T_e [OIII], T_e [OII], and T_e [SII] by combining our data in the red with our data in the blue. Regarding T_e [SIII], most of the observed HII galaxies show values that are slightly higher than those predicted from T_e [OIII] by photoionization models. This effect can be especially important for the high-excitation objects.

We derived the total S/H abundance for the 34 objects in the sample. Total S/H abundance was calculated directly using the electron temperature T_e [SIII] in 22 HII galaxies, for which the O/H abundance was obtained directly from the observations using T_e [OIII]. For the rest of the objects total S/H abundances were computed using the empirical abundance indicator S_{23} .

A comparative study was performed on the reliability of S_{23} and R_{23} as abundance indicators. No systematic variation in derived S/H with the excitation degree of the HII regions was found. That means that S_{23} is not sensitive to ionization effects, at first order, making it a robust empirical abundance indicator.

The comparison between η' and S_{23} parameters for our sample indicates that harder ionizing spectra are found in the HII galaxies with lower gaseous metallicity. Comparing the ionic ratios O^+/O^{++} and S^+/S^{++} with the predictions of single-star photoionization models, we note that a large fraction of galaxies in our sample are probably ionized by very hard spectra. This result points out that extra heating sources might exist, as has been suggested by recent works (Stasińska & Schaerer 1999; I05).

Finally, we presented a study of the abundance of S/H as a function of O/H in low-metallicity environments. Our data, together with other studies of S/H based upon the near-IR [SIII] lines, are consistent with the conclusion that S/O remains constant as O/H varies among the sample of HII galaxies. The scatter in S/O (due mainly to observational errors) is still large to constrain the degree of variation in S/O over the whole O/H abundance range. The assumption that the S/O ratio remains

constant at all abundances is still an open question that should be explored further.

Acknowledgements. C.K wishes to thank the Conselho Nacional de Desenvolvimento Científico e Tecnológico (CNPq-Brasil) for a grant and the Consejo Superior de Investigaciones Científicas (CSIC-Spain) for an I3P fellowship. We thank the referee for useful suggestions. We thank H.Plana for carrying out part of the spectroscopic observations. We also thank E.Pérez, R.M.González-Delgado and D. Reverte Payá for their help in the initial stages of this project, and to Jorge Iglesias-Páramo for his fruitful comments and careful reading of the manuscript. This research was partially funded by project AYA2004-08260-C03-02 of the Spanish PNAYA.

References

- Baldwin, J.A., Spinrad, H., & Terlevich, R. 1982, MNRAS, 198, 535
- Barker, T. 1980, ApJ, 240, 99
- Bresolin, F., Garnett, D.R., & Kennicutt, R.C. 2004, ApJ, 615, 228
- Bresolin, F., Kennicutt, R.C., & Garnett, D.R. 1999, ApJ, 510, 104
- Cairós, L.M., Caon, N., Vílchez, J.M., et al. 2001, ApJS, 136, 393
- Denicoló, G., Terlevich, R., & Terlevich, E. 2002, MNRAS, 330, 69
- Dennefeld, M. & Stasińska, G. 1983, A&A, 118, 234
- Díaz, A.I., & Pérez-Montero, E. 2000, MNRAS, 312, 130
- Díaz, A.I., Terlevich, E., Pagel, B.E.J., Vílchez, J.M., & Edmunds, M.G. 1987, MNRAS, 226, 19
- Edmunds, M.G., & Pagel, B.E.J. 1984, MNRAS, 211, 507
- Ferland, G.J., 2002, Univ. Kentucky Internal Report, HAZY: a brief introduction to CLOUDY
- Garnett, D.R. 1992, AJ, 103, 1330
- Garnett, D.R. 1989, ApJ, 345, 282 (G89)
- Izotov, Y.I., Stasińska, G., G. Meynet, Guseva, N.G., & Thuan, T.X. 2005, A&A, [astro-ph/0511644] (I05)
- Hoyos, C., & Díaz, A.I. 2006, MNRAS, 365, 454
- Kehrig, C., Telles, E. & Cuisinier, F., 2004, AJ, 128, 1141
- Kennicutt, R.C., Bresolin, F., French, H., & Martin, P. 2000, ApJ, 537, 589
- Leitherer, C., et al. 1999, ApJS, 123, 3
- Lodders, K. 2003, ApJ, 591, 1220L
- Martín-Hernández, N.L., et al. 2002, A&A, 381, 606
- Massey, P., Bresolin, F., Kudritzki, R.P., Puls, J., & Pauldrach, A.W.A. 2004, ApJ, 608, 1001
- McCall, M.L., Rybski, P.M. & Shields G.A. 1985, ApJS, 57, 1
- McGaugh, S.S. 1991, ApJ, 380, 140
- Mendoza, C., & Zeppen, C.J. 1982, MNRAS, 199, 1025
- Meynet, G., & Maeder, A. 2002, A&A, 390, 561
- Oey, M.S., & Shields, J.C. 2000, ApJ, 539, 687
- Oey, M.S., Dopita, M.A., Shields, J.C., & Smith, R.C. 2000, ApJS, 128, 511
- Osterbrock, D.E. 1989, Astrophysics of Gaseous Nebulae and Active Galactic Nuclei (Mill Valley: University Science Books)
- Pagel, B.E.J. 1997, Nucleosynthesis and Chemical Evolution of Galaxies, Cambridge, UK: Cambridge University Press

- Pagel, B.E.J., Edmunds, M.G., Blackwell, D.E., et al. 1979, MNRAS, 189, 95
- Paturel, G., Petit, C., Prugniel, P., et al. 2003, A&A, 412, 45
- Pérez-Montero, E., Díaz, A.I., Vílchez, J.M. & Kehrig, C. 2006, A&A, 449, 193 (PM06)
- Pérez-Montero, E., & Díaz, A.I. 2005, MNRAS, 361, 1063 (PMD05)
- Pérez-Montero, E. & Díaz, A.I. 2003, MNRAS, 346, 213 (PMD03)
- Pilyugin, L.S., Vílchez, J.M., & Contini, T. 2004, A&A, 425, 849
- Pilyugin, L.S. 2001, A&A, 369, 594
- Stasińska, G., & Schaerer, D. 1999, A&A, 351, 71
- Schaerer, D., & de Koter, A. 1997, A&A, 322, 598
- Searle, L., & Sargent, W.L.W. 1972, ApJ, 173, 25
- Storey, P.J., & Hummer, D.G. 1995, MNRAS, 272, 41
- Shaw, R.A., & Dufour, R.J. 1994, ASP Conf.Ser.61: Astronomical Data Analysis Software and Systems III, 61, 327
- Tayal, S.S., & Gupta, G.P. 1999, ApJ, 526, 544
- Telles, J.E. 1995, Ph.D. Thesis
- Terlevich, R., Melnick, J., Masegosa, J., Moles, M., & Copetti, M.V.F. 1991, A&AS, 91, 285
- Thuan, T.X., & Izotov, Y.I. 2005, ApJS, 161, 240
- Vacca, W.D., Cushing, M.C., & Rayner, J.T. 2003, PASP, 115, 389
- Van Zee, L., Salzer, J.J., Haynes, M.P., O'Donoghue, A.A., & Balonek, T.J. 1998, AJ, 116, 2805
- Vermeij, R., Damour, J.M., van der Hulst, J.M. & Baluteau, J.P. 2002, A&A, 390, 649.
- Vílchez, J.M., & Iglesias-Páramo, J. 2003, ApJS, 145, 225
- Vílchez, J.M., & Iglesias-Páramo, J. 1998, ApJ, 508, 248
- Vílchez, J.M. & Esteban, C. 1996, MNRAS, 280, 720
- Vílchez, J.M., Pagel, B.E.J., Díaz, A.I., et al. 1988, MNRAS, 235, 633
- Vílchez, J.M. & Pagel, B.E.J. 1988, MNRAS, 231, 257
- Whitford, A.E. 1958, AJ, 63, 201
- Woosley, S.E. & Weaver, T.A. 1995, ApJS, 101, 181